Studies of the magnetic structure at the ferromagnet–antiferromagnet interface

A. Scholl, [a]* F. Nolting, [a,b] J. Stöhr, [b,c] J. Lüning, [b] J. W. Seo, [d,e] J.-P. Locquet, [e] J. Fompeyrine, [e] S. Anders, [a,c] H. Ohldag [a,b,f] and H. A. Padmore [a]

[a]Advanced Light Source, 1 Cyclotron Road, Lawrence Berkeley National Laboratory, Berkeley, CA 94720, USA, [b]Stanford Synchrotron Radiation Laboratory, PO Box 20450, Stanford, CA 94309, USA, [c]IBM Research Division, Almaden Research Center, 650 Harry Road, San Jose, CA 95120, USA, [d]Institute de Physique, University of Neuchâtel, CH-2000 Neuchâtel, Switzerland, [e]IBM Research Division, Zürich Research Laboratory, CH-8803, Rüschlikon, Switzerland, and [f]Institute of Applied Physics, University of Düsseldorf, Universitätsstr. 1, 40225 Düsseldorf, Germany. E-mail: a_scholl@lbl.gov

Antiferromagnetic layers are a scientifically challenging component in magnetoelectronic devices, such as magnetic sensors in hard-disk heads, or magnetic random-access memory (RAM) elements. In this paper, it is shown that photoelectron emission microscopy (PEEM) is capable of determining the magnetic structure at the interface of ferromagnets and antiferromagnets with high spatial resolution (down to 20 nm). Dichroism effects at the L edges of the magnetic $3d$ transition metals, using circularly or linearly polarized soft X-rays from a synchrotron source, give rise to a magnetic image contrast. Images, acquired with the PEEM2 experiment at the Advanced Light Source, show magnetic contrast for antiferromagnetic $LaFeO_3$, microscopically resolving the magnetic domain structure in an antiferromagnetically ordered thin film for the first time. Magnetic coupling between $LaFeO_3$ and an adjacent Co layer results in a complete correlation of their magnetic domain structures. From field-dependent measurements, a unidirectional anisotropy resulting in a local exchange bias of up to 30 Oe in single domains could be deduced. The elemental specificity and the quantitative magnetic sensitivity render PEEM a perfect tool to study magnetic coupling effects in multilayered thin-film samples.

Keywords: magnetic properties; ferromagnet–antiferromagnet interface; photoelectron emission microscopy (PEEM); X-ray magnetic dichroism; thin films.

1. Introduction

Anisotropy, confinement and interface effects completely alter the magnetic properties of thin magnetic films, enabling the engineer to design improved magnetic materials with novel properties. The surface and interface anisotropy is an important factor influencing the magnetic symmetry of thin films (Gradmann, 1991; Stöhr, 1999). Dimensionality effects control ordering parameters, such as the Curie temperature in ferromagnets or the Néel temperature in antiferromagnets that have thicknesses approaching monolayer thickness (Alders *et al.*, 1998; Schneider *et al.*, 1990). Magnetic exchange coupling and spin transport at interfaces are responsible for technologically important effects, such as magnetic interlayer coupling, spin-tunneling and giant magnetoresistance (Fert *et al.*, 1995). These effects are applied in technologically relevant devices, such as magnetic sensors in hard-disk read heads or magnetic random access memory (MRAM), generally referred to as spintronics applications. X-ray techniques are widely used, because of their high and quantitative magnetic sensitivity, utilizing magnetic X-ray dichroism, and their elemental specificity (Kortright *et al.*, 1999). The variable probing depth of X-ray absorption by variation of the detected particles, such as transmitted or reflected photons, fluorescence photons, low-energy secondary electrons or photoelectrons, allows the study of surface, interface or bulk effects.

In particular, we have investigated the magnetic structure of antiferromagnetic thin films and the phenomenon of exchange bias at the ferromagnet–antiferromagnet interface using X-ray photoelectron emission microscopy (PEEM) (Nolting *et al.*, 2000; Scholl *et al.*, 2000; Stöhr *et al.*, 1999). Exchange bias or magnetic pinning occurs when a ferromagnetic and an antiferromagnetic layer are grown adjacent to each other in an applied magnetic field, resulting in a unidirectional magnetic anisotropy or a shift of the magnetic hysteresis loop of the ferromagnet (Berkowitz & Takano, 1999; Nogues & Schuller, 1999). Pinned magnetic layers serve as magnetic reference layers in magnetoelectronic devices, utilizing the insensitivity of antiferromagnets to magnetic fields. The microscopic origin of exchange bias is still poorly understood, largely owing to the lack of techniques capable of providing information about the arrangement of spins at ferromagnet–antiferromagnet interfaces.

2. Experiment

Samples consisting of an antiferromagnetic $LaFeO_3$ layer and a ferromagnetic Co layer, grown on an $SrTiO_3$ substrate, were investigated. The $LaFeO_3$ films were grown in an oxide molecular beam epitaxy (MBE) system by means of a block-by-block growth method (Locquet *et al.*, 1994) at 1020 K under a beam of atomic oxygen and a partial O_2 pressure of 5×10^{-6} torr (1 torr = 133.32 Pa). This method yields high-quality epitaxic films (Locquet *et al.*, 1998). The Co layers were grown on $LaFeO_3$ by MBE without breaking the vacuum and were protected from oxidation by a Pt coating of thickness 10 Å.

The experimental setup is shown in the top-right part of Fig. 1 (Anders *et al.*, 1999). Monochromated X-rays from bending-magnet beamline 7.3.1.1 of the Advanced Light Source illuminate the sample under an angle of incidence of 30°. The X-ray polarization can be easily varied from right circular to left circular and linear by moving an aperture in the beamline. We have exploited the polarization dependence of X-ray absorption in magnetic materials, investigating the antiferromagnet $LaFeO_3$ using X-ray magnetic linear dichroism (XMLD) and the ferromagnet Co using X-ray magnetic circular dichroism (XMCD). The electric field vector for linearly polarized light lies in the sample plane. The all electrostatic PEEM2 microscope images low-energy secondary photoelectrons from the sample with magnification onto a phosphor screen, which is read by a charge-coupled device (CCD) camera. The spatial resolution of PEEM2 is limited by chromatic aberrations to 20 nm. A small electromagnet mounted on the sample puck was used to magnetize the sample in fields of up to 25 mT parallel to the surface.

3. Results

Our experiments make use of the large XMLD effect previously observed for α-Fe_2O_3 (Kuiper *et al.*, 1993). The magnetic contribution to the temperature and polarization dependence of the Fe L-edge resonance intensity is proportional to $(3\cos^2\theta - 1)\langle M^2\rangle_T$, where θ is the angle between the X-ray polarization vector $\vec{\mathbf{E}}$ and the magnetic axis $\overleftrightarrow{\mathbf{A}}$, and $\langle M^2\rangle_T$ is the expectation value of the square of the magnetic moment (Alders *et al.*, 1998; Stöhr *et al.*, 1999). Thus, X-ray absorption spectroscopy is sensitive to the orientation of the anti-

ferromagnetic axis $\overleftrightarrow{\mathbf{A}}$ within an antiferromagnetic domain relative to the X-ray polarization. In particular, peak *A* of the Fe L_2 edge at 721.5 eV is larger than peak *B* at 723.2 eV (see Fig. 1 inset) for $\vec{\mathbf{E}} \perp \overleftrightarrow{\mathbf{A}}$ and smaller for $\vec{\mathbf{E}} \parallel \overleftrightarrow{\mathbf{A}}$. The antiferromagnetic domains can be directly observed by combining XMLD spectroscopy with PEEM microscopy; that is, by dividing a PEEM image acquired at 723.2 eV (image *B*) by one obtained at 721.5 eV (image *A*). The divided XMLD image *B*/*A* in Fig. 1 shows the antiferromagnetic domain structure of $LaFeO_3$, with domains with $\vec{\mathbf{E}} \parallel \overleftrightarrow{\mathbf{A}}$ appearing brighter than domains with $\vec{\mathbf{E}} \perp \overleftrightarrow{\mathbf{A}}$.

The angular dependence of the XMLD image contrast is depicted in Fig. 2. Two $SrTiO_3$ substrate crystals were joined macroscopically at the (110) and (010) faces, leading to a 45° rotation of the lattice around the surface normal. Crystallographic twins in each half have an orthogonal orientation of the crystallographic *c* axes, which lie in the sample plane, observed by transmission electron microscopy and X-ray diffraction. The crystallographic *c* axes of these twins are oriented along the diagonals on the left, whereas they are oriented vertical and horizontal on the right. Apparently, magnetocrystalline anisotropy forces the antiferromagnetic axis $\overleftrightarrow{\mathbf{A}}$ parallel or perpendicular to the crystallographic *c* axis, explaining the vanishing contrast on the left [$\measuredangle(\overleftrightarrow{\mathbf{A}}, \vec{\mathbf{E}}) = \pm 45°$] and the strong contrast on the right [$\measuredangle(\overleftrightarrow{\mathbf{A}}, \vec{\mathbf{E}}) = 0$ or 90°]. The antiferromagnetic configuration is displayed at the bottom of Fig. 2. From an analysis of non-spatially-resolved spectroscopic data (not shown), we deduce that $\overleftrightarrow{\mathbf{A}}$ is inclined by 45° to the sample surface. Since in our experimental geometry $\vec{\mathbf{E}}$ lies in the surface plane, we cannot distinguish domains in which the axis $\overleftrightarrow{\mathbf{A}}$ is rotated by 180° about the surface normal. Thus we only observe two of the four antiferromagnetic domains that have to exist by symmetry.

Magnetic exchange coupling at the interface between an antiferromagnet and a ferromagnet is expected to cause corresponding domain configurations in both layers. We have investigated the domain structure in a Co wedge, grown on top of $LaFeO_3$ with a thickness ranging from 8 Å up to 25 Å, which was coated with Pt with a thickness of 10 Å to prevent oxidization. The probing depth of photoelectron emission microscopy using low-energy secondary electrons (20–50 Å) permits imaging of the $LaFeO_3$ and Co layers at the same time. The elemental specificity of X-ray absorption techniques furthermore allows distinguishing both layers, by acquiring images at the characteristic absorption resonances. In Fig. 3, the Co ferromagnetic and $LaFeO_3$ antiferromagnetic domain structure, acquired at exactly the same position, are shown together. The Co ferromagnetic configuration was imaged by applying X-ray magnetic circular dichroism (XMCD) contrast, by dividing images acquired at the Co L_3 edge and at the Co L_2 edge using circularly polarized X-rays. The $LaFeO_3$ antiferromagnetic configuration was imaged using

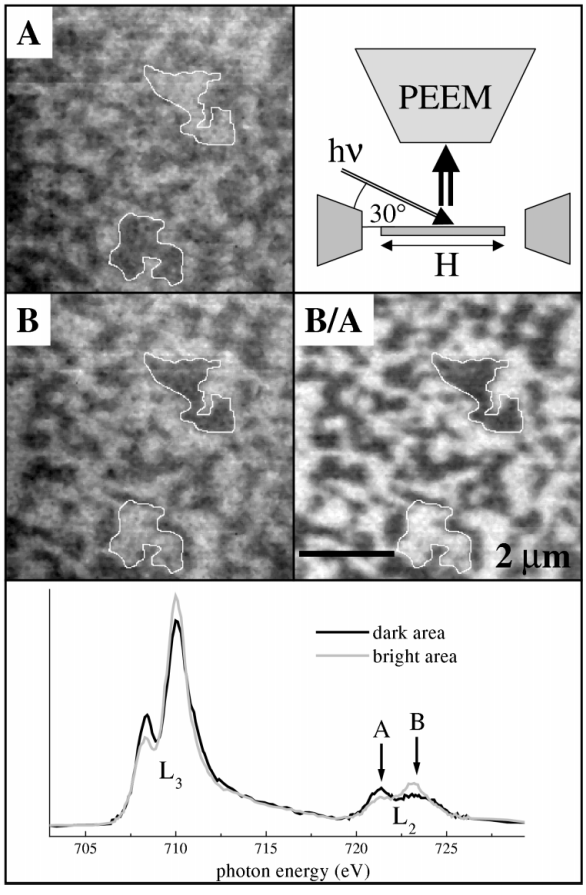

Figure 1
Images acquired at 721.5 eV (*A*) and 723.2 eV (*B*) at the Fe L_2 edge using linearly polarized X-rays show the antiferromagnetic domain structure of $LaFeO_3$. The domain contrast at energy *B* is reversed compared with that at *A*. In the divided image *B*/*A*, referred to as the XLMD image, contrast of non-magnetic origin (topography, chemical composition) is suppressed. Local spectra measured within a dark and a bright domain show the origin of the image contrast: the branching ratio between two multiplet peaks at the L_2 edge changes, because of the different angle between the X-ray polarization vector and the antiferromagnetic axis in each domain. The measurement geometry is also shown.

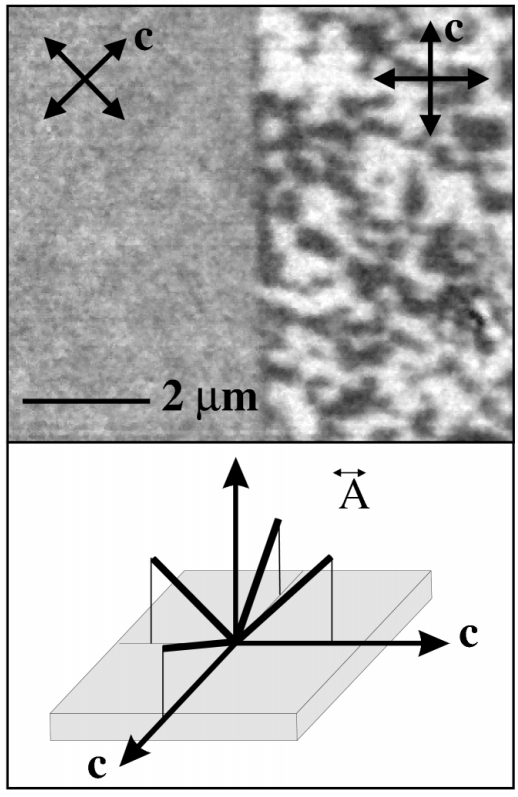

Figure 2
The domain structure at the junction of an $LaFeO_3$ bicrystal is shown. The crystal lattice is rotated by 45° at the boundary, indicated by black arrows, accompanied by a similar rotation of the antiferromagnetic axis. The photon polarization is horizontal. The relation between the magnetic configuration and the crystallographic structure is shown at the bottom.

XMLD contrast, as explained above. The images show a clear correspondence of the domain structures. On the left, two colors appear in the $LaFeO_3$ magnetic image, representing the two antiferromagnetic domains with orthogonal orientation of the antiferromagnetic axis that we are able to distinguish. Strong contrast arises between domains with the antiferromagnetic axis $\vec{\mathbf{A}}$ parallel and perpendicular to the electric field vector $\vec{\mathbf{E}}$, which is horizontal. Three colors in the Co XMCD image on the right correspond to four different directions of the magnetization vector $\vec{\mathbf{M}}$. Using circularly polarized light, ferromagnetic domains with an opposite projection of $\vec{\mathbf{M}}$ on the X-ray polarization $\vec{\sigma}$ can be distinguished. They appear bright in case of parallel orientation ($\vec{\mathbf{M}}$ down) and dark in case of antiparallel orientation ($\vec{\mathbf{M}}$ up). Domains with $\vec{\mathbf{M}}$ pointing to the left and the right, orthogonal to the polarization $\vec{\sigma}$, appear in the same gray shade and are not differentiated in this image. These domains were resolved by a 90° rotation of the sample (not shown). Comparison of the in-plane projections of the antiferromagnetic axis and the ferromagnetic spin directions, illustrated above the images, reveals that the ferromagnetic Co spins are always aligned parallel or antiparallel to the in-plane projection of the antiferromagnetic axis. The correlation revealed by Fig. 3 is of magnetic rather than crystallographic origin since the Co layer is polycrystalline. The magnetic alignment of the Co domains, which exhibit an in-plane easy axis, must therefore be caused by a coupling to uncompensated spins at the $LaFeO_3$ surface with an in-plane component parallel to the in-plane projection of the antiferromagnetic axis. Experiments to image this ferromagnetic component directly were unsuccessful on this system, probably because of their small concentration or magnitude.

In Fig. 4, the Co ferromagnetic domain structure and the $LaFeO_3$ antiferromagnetic domain structure are shown for different Co thicknesses. All images show magnetic domains of comparable size and the described correspondence between the magnetic configuration of the ferromagnetic and the antiferromagnetic layer. As expected, the intensity originating from the buried $LaFeO_3$ layer decreases with Co thickness, whereas the intensity from the Co layer increases. However, imaging through a cap layer of 30 Å thickness is still possible. The variation of the image contrast does not signify a modification of the magnetic moment with Co thickness. It is caused by the change of the peak-jump to background ratio of the Fe or Co resonances with Co layer thickness.

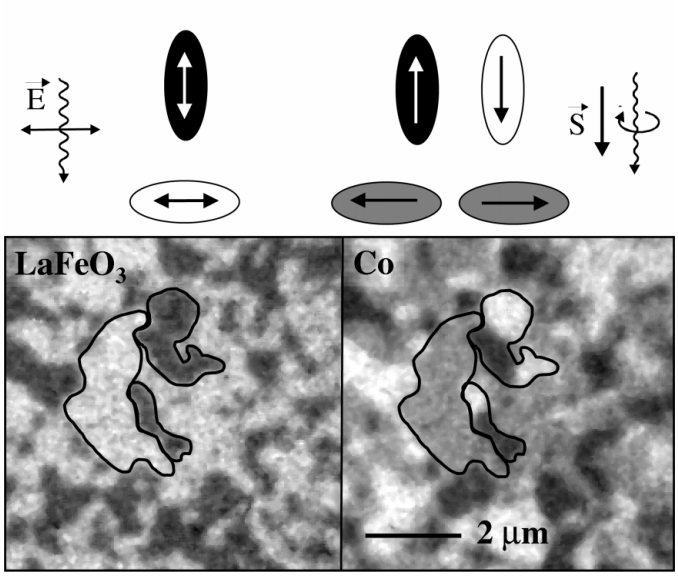

Figure 3
Antiferromagnetic domains in $LaFeO_3$ (left) and ferromagnetic domains in Co (right) were imaged exactly at the same position. Different colors signify a different direction of the magnetic vector, as indicated above the images.

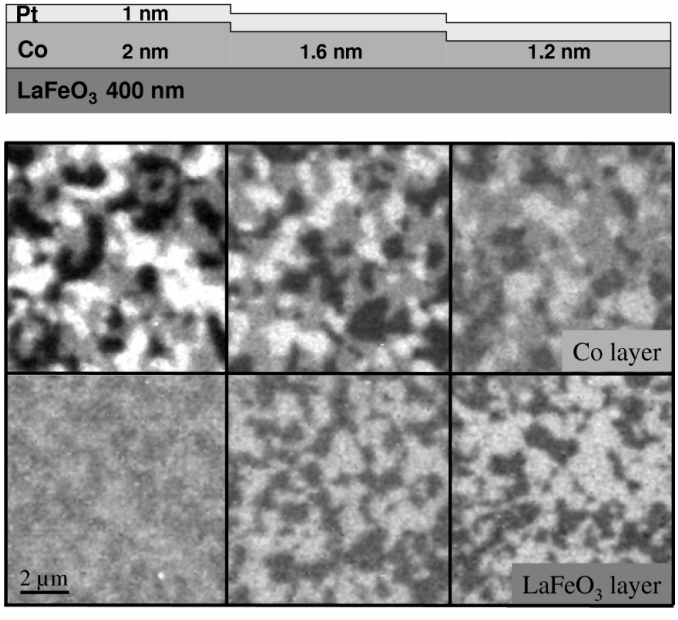

Figure 4
Thickness dependence of the Co (top) and the $LaFeO_3$ (bottom) domain contrast in an $LaFeO_3$/Co bilayer, coated with Pt.

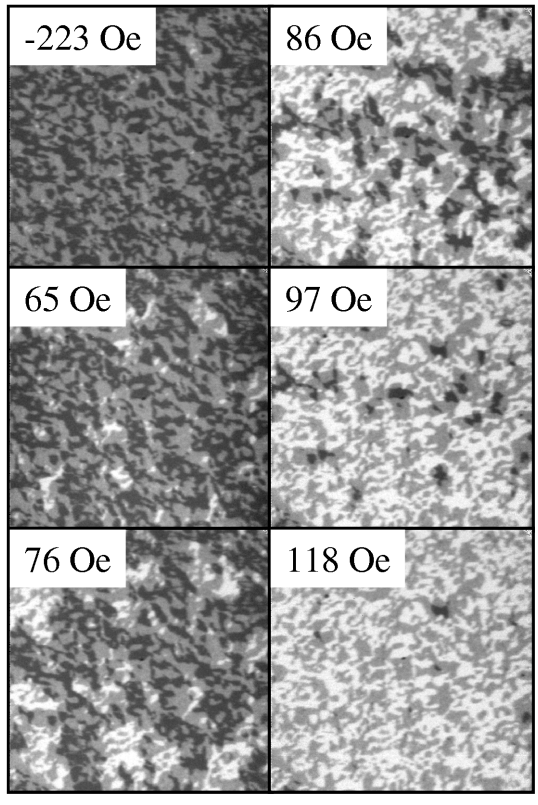

Figure 5
XMCD images of the Co domain structure. The images were acquired in remanence after applying magnetic fields in the sample plane.

Investigations of the magnetization-reversal process in the ferromagnetic layer have been carried out to quantify the coupling strength at the antiferromagnet–ferromagnet interface. A sequence of Co XMCD images was acquired after applying various magnetic fields (a subset is shown in Fig. 5). The measurements were performed on a 25 Å $Co/LaFeO_3(001)$ sample. The field was applied along the in-plane projection of the X-ray propagation (see Fig. 1) and microscopic XMCD images were acquired in zero field, because of the deflection of electrons in a magnetic field. The images show that the magnetization reversal occurs by the switching of individual domains, the magnetization direction and shape of which are defined by exchange coupling to the $LaFeO_3$ layer, and not by domain-wall motion. The images also reveal a strong uniaxial anisotropy of the Co domains. Only Co domains that are coupled to $LaFeO_3$ domains with a projection of the antiferromagnetic axis parallel to the field can be reversed (black to white), while orthogonal Co domains (gray) follow a hard axis loop and remain unchanged even after applying a field of more than 200 Oe. We furthermore observe a local unidirectional magnetic anisotropy of single Co domains: a local exchange bias. Local remanent hysteresis loops (Fig. 6), calculated from the field-dependent XMCD contrast in a sequence of images, show a repeatable loop shift of up to 30 Oe and more in single domains. This local bias is attributed to a surplus of uncompensated interface spins in the individual antiferromagnetic domains, which are frozen in after growth. Spatially averaged, the bias effects of individual domains cancel out, leading to the non-shifted averaged hysteresis loop, also shown in Fig. 6. The averaged loop exhibits only half of the XMCD brightness change because the orthogonal gray domains constitute half of the signal but do not switch. The lack of bias in the averaged loop is expected, because the studied sample was not set in a magnetic field. The setting procedure would shift the balance of the microscopically biased domains, resulting in a preferred macroscopic spin direction, *i.e.* macroscopic exchange bias.

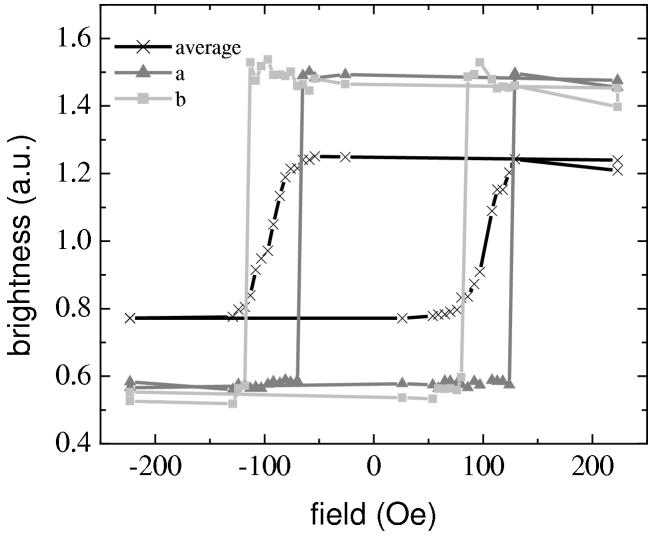

Figure 6
Remanent hysteresis loops calculated from the XMCD intensity in two selected domains, which have opposite bias. The average loop shows the XMCD intensity averaged over a multidomain region.

4. Conclusions

We have determined the magnetic structure of an antiferromagnet/ferromagnet bilayer, in particular of the system $Co/LaFeO_3$. The antiferromagnetic domain structure in a thin-film sample has been resolved for the first time, using X-ray photoelectron emission microscopy. We have also investigated the magnetic interaction at the $Co–LaFeO_3$ interface. Magnetic exchange coupling across the interface causes a clear correspondence of the ferromagnetic and the antiferromagnetic domain structure in both layers. Investigation of the magnetization-reversal process allowed the quantification of the local bias field in single domains. We believe that X-ray absorption microscopy may hold the key to a definite understanding of the ferromagnet–antiferromagnet exchange bias phenomenon.

The sample preparation and characterization was carried out at the IBM research centers in Almaden, San Jose, USA, and Zürich, Switzerland. The authors thank H. Siegwart, E. Fullerton, M. F. Toney and M. R. Scheinfein who contributed to this work. This work was supported by the Director, Office of Basic Energy Sciences, of the US Department of Energy. JWS and FN acknowledge support by the Swiss National Science Foundation.

References

Alders, D., Tjeng, L. H., Voogt, F. C., Hibma T., Sawatzky, G. A., Chen, C. T., Vogel, J., Sacchi, M. & Iacobucci, S. (1998). *Phys. Rev. B*, **57**, 11623–11631.
Anders, S., Padmore, H. A., Duarte, R. M., Renner, T., Stammler, T., Scholl, A., Scheinfein, M. R., Stöhr, J., Seve, L. & Sinkovic, B. (1999). *Rev. Sci. Instrum.* **70**, 3973–3981.
Berkowitz, A. E. & Takano, K. (1999). *J. Magn. Magn. Mater.* **200**, 552–570.
Fert, A., Grünberg, P., Barthelemy, A., Petroff, F. & Zinn, W. (1995). *J. Magn. Magn. Mater.* **140–144**, 1–8.
Gradmann, U. (1991). *J. Magn. Magn. Mater.* **100**, 481–496.
Kortright, J. B., Awschalom, D. D., Stöhr, J., Bader, S. D., Idzerda, Y. U., Parkin, S. S. P., Schuller, I. K. & Siegmann, H. C. (1999). *J. Magn. Magn. Mater.* **207**, 7–44.
Kuiper, P., Searle, B. G., Rudolf, P., Tjeng, L. H. & Chen, C. T. (1993). *Phys. Rev. Lett.* **70**, 1549–1552.
Locquet, J. P., Catana, A., Machler, A. E., Gerber, C. & Bednorz, J. G. (1994). *Appl. Phys. Lett.* **64**, 372–374.
Locquet, J. P., Perret, J., Fompeyrine, J., Machler, E., Seo, J. W. & Van Tendeloo, G. (1998). *Nature (London)*, **394**, 453–456.
Nogues, J. & Schuller, I. K. (1999). *J. Magn. Magn. Mater.* **192**, 203–232.
Nolting, F., Scholl, A., Stöhr, J., Seo, J. W., Fompeyrine, J., Siegwart, H., Locquet, J. P., Anders, S., Lüning, J., Fullerton, E. E., Toney, M. F., Scheinfein, M. R. & Padmore, H. A. (2000). *Nature (London)*, **405**, 767–769.
Schneider, C. M., Bressler, P., Schuster, P., Kirschner, J., de Miguel, J. J. & Miranda, R. (1990). *Phys. Rev. Lett.* **64**, 1059–1062.
Scholl, A., Stöhr, J., Lüning, J., Seo, J. W., Fompeyrine, J., Siegwart, H., Locquet, J. P., Nolting, F., Anders, S., Fullerton, E. E., Scheinfein, M. R. & Padmore, H. A. (2000). *Science*, **287**, 1014–1016.
Stöhr, J. (1999). *J. Magn. Magn. Mater.* **200**, 470–497.
Stöhr, J., Scholl, A., Regan, T. J., Anders, S., Lüning, J., Scheinfein, M. R., Padmore, H. A. & White, R. L. (1999). *Phys. Rev. Lett.* **83**, 1862–1865.